

Atomic Transition Probabilities: Past and Future Measurements

Lorenzo J. Curtis

Department of Physics and Astronomy, University of Toledo, Ohio 43606, USA

Received January 3, 2005; accepted March 1, 2005

PACS number: 32.70 Cs

Abstract

The study of atomic and ionic lifetimes and transition probabilities has undergone a period of intense activity, facilitated largely by the application of the technique of Beam-Foil Spectroscopy. This area is now a mature field of study (having been pursued for 40 years), and has provided much new data, elucidated fundamental atomic processes, and furthered applications in many fields. However, technical advances have now broadened the field to permit new types of measurements of unprecedented accuracy and scope. Thus, this occasion offers an appropriate opportunity to review some of the successful applications of the method, to survey the present state of knowledge, and to indicate areas that hold promise for future research.

1. Introduction

In recent years, substantial progress has been made in the measurement of atomic meanlives, both in the level of precision of the individual measurements [1], and in their extension both to highly complex many-electron systems and to highly charged ions along isoelectronic sequences [2]. For neutral and few times ionized systems, laser methods using selective excitation can now provide high precision, and ion trap methods allow measurements to be made for long-lived metastable states. Complementing this, the excitation of a fast ion beam by a thin foil provides access to the spectrum of virtually any ionization stage of any element. Moreover, technical improvements have greatly enhanced the precision and reliability of beam-foil measurements. The application of these techniques has produced a wealth of atomic meanlife data, much of which has been systematized and parametrized in ways that not only yield accurate extrapolative and interpolative predictions, but also reveal linearities and other regularities that provide useful dynamical and conceptual insights [3]. However, these methods require that meanlife and branching fraction measurements be combined to obtain oscillator strengths, and branching fraction data are virtually non-existent for multiply charged ions.

The application of these methods shows great promise in meeting the desirable goal of providing a comprehensive and reliable base of atomic structure data that spans all atoms and ions, but a number of challenges still remain. Here the present status of these measurements will be reviewed, and some of the significant problems that must be addressed will be discussed.

2. Fast ion beam methods

Foil excitation of a fast ion beam has many unusual features. Since this excitation takes place in a dense environment within the foil and at its exit surface, it produces broad excitation, including high Rydberg states, multiply-excited states, and metastable states. In contrast, the decay occurs in an extremely tenuous plasma, and is thus free of fields, collisions, and radiation trapping. The light source is not only time-resolved, but also exhibits coherent

and anisotropic excitation, permitting classes of experiments not accessible to many other types of light sources. Techniques have been developed by which the Doppler broadening is narrowed by refocusing of the dispersion optics to a moving light source, thus minimizing blending effects. Cascade repopulation can be reliably accounted for by methods that exploit joint analysis of correlations among sequentially populated decay curves. Position sensitive detectors now permit simultaneous multiplexed detection of many different decay curves. This leads to a great increase in detection efficiency, which is important because of the low light levels that occur due to the low density of the source. It also permits deblending by examination of lifetime content as a function of wavelength within a line profile. Moreover, the simultaneous measurement causes many sources of systematic uncertainty to cancel in the differential measurement of relative meanlives. These technical developments have greatly enhanced the accuracy, reliability, and applicability of the method. If applied at the present state-of-the-art, the method can provide comprehensive data that could be used to characterize the complete data base.

3. Semiempirical systematizations

Much progress in the evaluation, interpolation and extrapolation of atomic transition probability rate data has been obtained through systematic studies along isoelectronic sequences [2]. For these purposes, the line strength factor S_{if} usually exhibits a much simpler isoelectronic variation than that of the transition probabilities or oscillator strengths. The quantity S_{if} can be deduced from the lifetime τ , the branching fraction B_{if} , the transition wavelength λ_{if} , and the upper level degeneracy g_i using the relationship

$$S_{if} = [\lambda_{if}(\text{\AA})/1265.38]^3 g_i B_{if} / \tau_i(\text{ns}). \quad (1)$$

It has been observed that this quantity, scaled (like the corresponding hydrogenlike value) by the square of the nuclear charge, has an almost linear dependence on a suitably chosen reciprocal screened charge. Thus large blocks of isoelectronic data can be parametrized by the fitting function

$$Z^2 S \approx S_0 + b/(Z - C_0), \quad (2)$$

where S_0 , b and C_0 are empirical constants. In this manner a relatively small number of precision lifetime measurements can be used to interpolatively predict line strengths for entire isoelectronic sequences. Examples of sequences that have been systematized by these methods will be described below.

3.1. Alkali-metallike sequences

Isoelectronic regularities in line strength data for complex atoms were first recognized [4] in the study of scaled line strengths

for $\Delta n = 0$ resonance transitions in alkali-metallike systems. For these systems, it has been discovered [5], not only that the isoelectronic variation can be linearized, but also that the semiempirical fitting parameter S_0 effectively matches the corresponding hydrogenic $\Delta n = 0$ value S_H . This quantity is given by

$$S_0 \rightarrow S_H \equiv 3n^2(n^2 - 1)g_i/4. \quad (3)$$

Expositions of the existing data bases for the Li, Na, Cu, and Ag sequences are shown in Fig. 1. The upper lines trace the $J \rightarrow \frac{3}{2}-\frac{1}{2}$ transitions and the lower lines trace the $J \rightarrow \frac{1}{2}-\frac{1}{2}$ transitions. The solid diamond symbols indicate the hydrogenic values. In these systems the $ns-np$ resonance transitions are unbranched, so $B_{if} = 1$ and the line strengths are determined directly from the measured lifetimes. If the linearity of Eq. (2) is valid, then accurate measurements for the lifetimes of a few members of the sequence at low stages of ionization can be interpolated to the hydrogenic limit at high Z , providing accurate estimates for all intervening ions.

While these expositions exhibit empirical linearities for low to medium degrees of ionization, the hydrogenlike value given in Eq. (3) is non-relativistically computed, and at very high Z this Schrödinger formulation would be expected to break down. Correspondingly, the solution to the Dirac equation for a pure $1/r$ potential is given by

$$Z^2 S = S_H \left[1 - \sum_i a_i (\alpha Z)^{2i} \right], \quad (4)$$

where S_H is given by Eq. (3) and a_i is a set of coefficients tabulated in Ref. [5]. An experimental test of this high Z behavior is available for the Li sequence, where the $2p \ ^2P_{1/2}$ lifetime has been measured for lithiumlike uranium [6]. This measurement falls considerably below the linear trend of the plot if no relativistic corrections are made, but the discrepancy disappears when the semiempirical exposition of Eq. (2) is modified to take into account the high Z behavior of the corresponding hydrogenlike system, using the fitting function

$$Z^2 S \left[1 - \sum_i a_i [\alpha(Z - C_0)]^{2i} \right]^{-1} \approx S_H + b/(Z - C_0). \quad (5)$$

With this modification, the formulation permits the existing data base to be used to accurately specify line strengths for the entire isoelectronic sequence. Moreover, the straight line empirical fits presented for the Li, Mg, Cu, and Ag sequences in Fig. 1 are virtually indistinguishable from the corresponding loci of recent *ab initio* calculations for these sequences [7, 8]. Thus the oscillator strengths of the lowest resonance transitions in the alkali-metallike sequences can now be considered as precisely known quantities.

However, even for these sequences much work remains to be done for the specification of transition probabilities between excited states. The transitions are not only branched (requiring branching fractions for their experimental specification), but their transition moments are also affected by strong cancellation effects (making their theoretical calculation difficult).

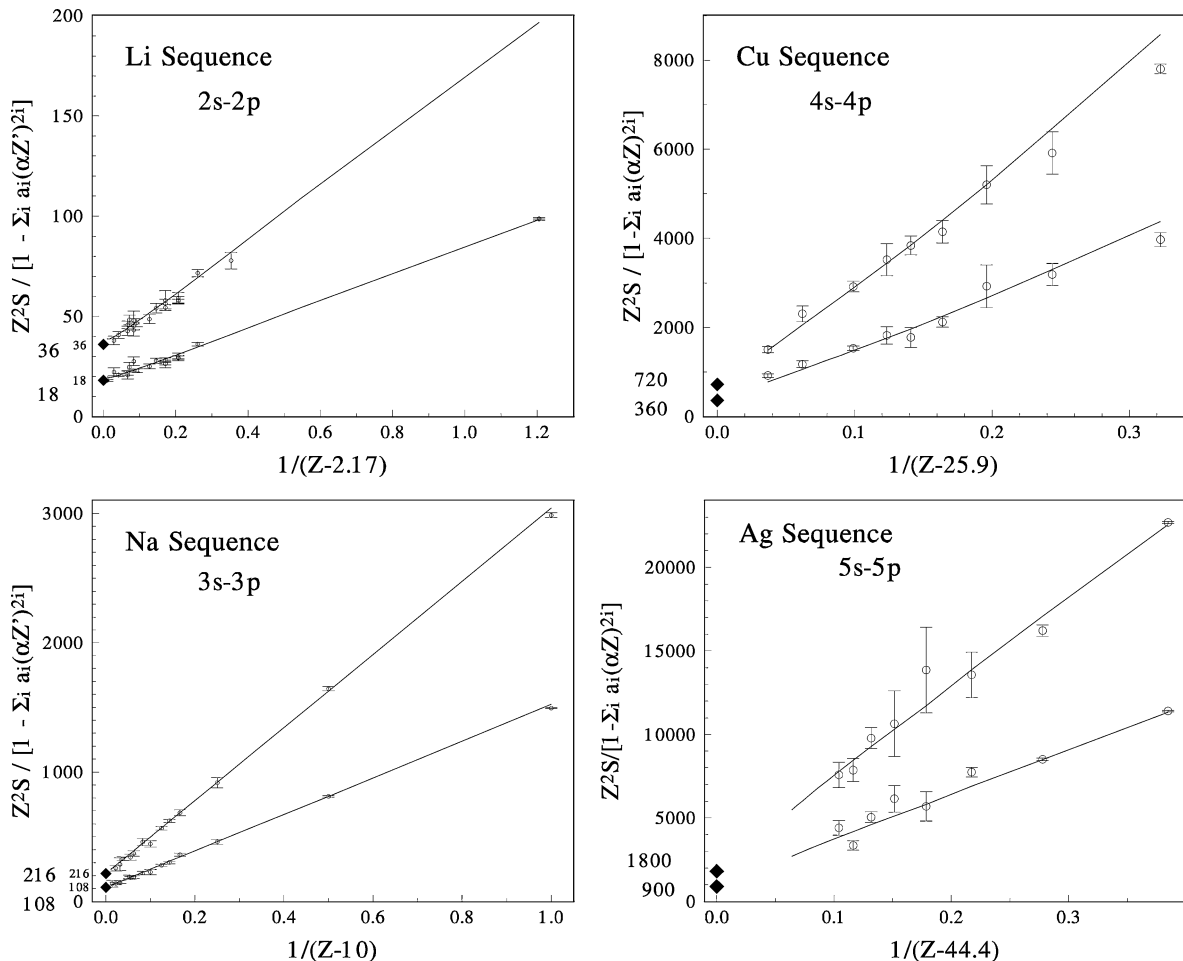


Fig. 1. Plot of scaled line strength vs reciprocal screened charge for the $ns-np$ transitions in the alkali-metallike Li, Na, Cu and Ag sequences.

3.2. Alkaline-earthlike sequences

In the case of systems in which two valence electrons (or one electron and one hole) occur in an otherwise closed shell core, a simple extension of this formalism has been developed that combines lifetime data for the resonance and intercombination lines. In systems such as $ns^2\text{-}nsn'p$ (and $np^6\text{-}np^5n's$), both the $^1S_0\text{-}^1P_1$ and $^1S_0\text{-}^3P_1$ transitions occur because intermediate coupling (IC) causes spin hybridization of the nominally singlet and triplet excited states. In the absence of significant configuration interaction (CI) effects, the IC amplitudes can be determined from spectroscopic energy level data and expressed in the form of a singlet-triplet mixing angle θ [9]. The measured lifetime data for the unbranched resonance and intercombination lines are first converted to line strengths $S(\text{Res})$ and $S(\text{Int})$ using Eq. (1), and then reduced to the effective values

$$S_r(\text{Res}) \equiv S(\text{Res})/\cos^2\theta, \quad (6)$$

$$S_r(\text{Int}) \equiv S(\text{Int})/\sin^2\theta, \quad (7)$$

from which the effects of intermediate coupling have been removed. Empirical plots of data that have been reduced in this way are shown in Fig. 2 for the unbranched (hence $B_{if} = 1$) $ns^2\text{-}nsn'p$ transitions in the Mg, Zn, Cd, and Hg sequences. Here both $J = 1$ levels tend to converge to values of S_H twice those predicted by Eq. (3) (consistent with the two equivalent ground-term electrons), which are indicated by the solid diamond symbols.

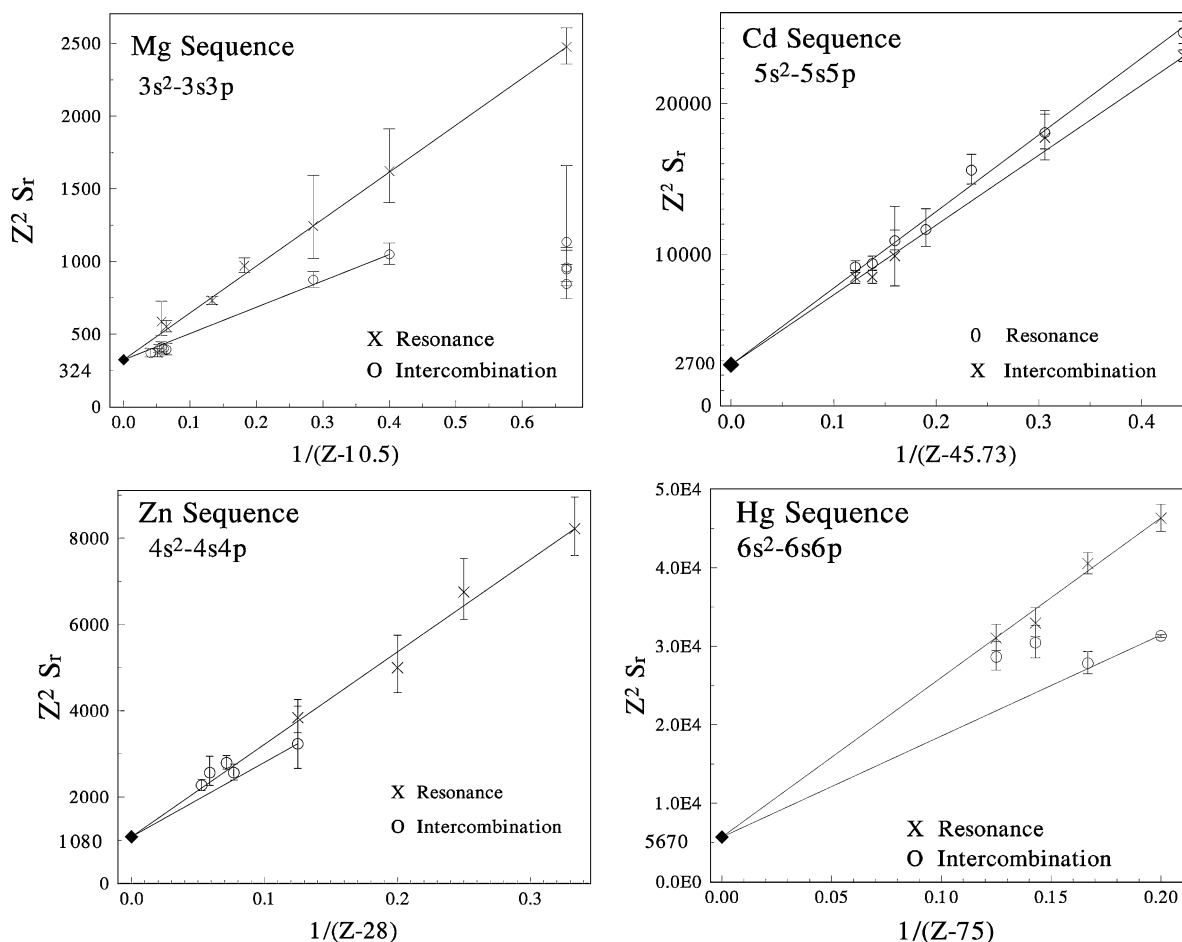


Fig. 2. Plot of scaled IC-reduced line strength vs reciprocal screened charge for the $ns^2\text{-}nsn'p$ transitions in the alkaline-earthlike Mg, Zn, Cd and Hg sequences.

If expressed in terms of $\cot(2\theta)$, the mixing angles also possess linear properties that permit their interpolation and extrapolation. This is illustrated on a log-log plot in Fig. 3. The linearity exhibited on this plot indicates that the mixing angles can be accurately represented by the expression

$$\cot(2\theta) \approx \cot(2\theta_{jj}) + D/(Z - C_1)^p, \quad (8)$$

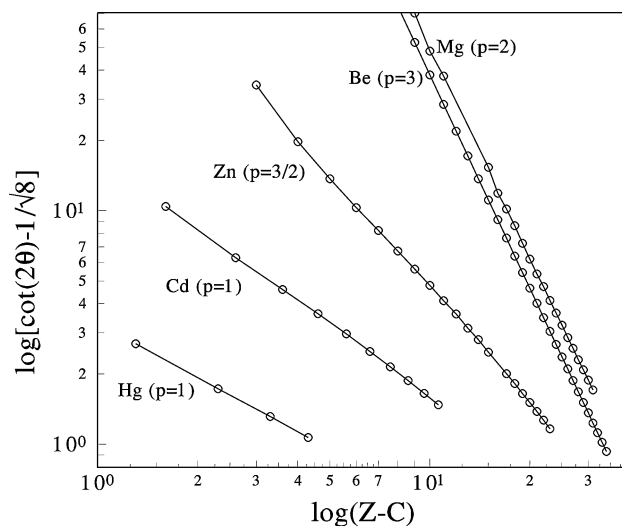


Fig. 3. Log-log plot of the singlet-triplet mixing factor $\cot(2\theta) - \cot(2\theta_{jj})$ vs screened charge for the alkaline-earthlike isoelectronic sequences.

where θ_{jj} is the value in the jj coupling limit ($1/\sqrt{8}$ for sp configurations) and D , C_1 and p are empirical fitting parameters. Since there are three energy splittings within an sp configuration that are described by two Slater parameters (G_1 and ζ_p) [9], the system is overdetermined. There are various ways to utilize this overdetermination to check the validity of the single configuration assumption.

Studies have been made [10] to characterize within this semiempirical formulation the relativistic differences that exist between the radial dipole matrix elements for the resonance and intercombination transitions. These indicate that, for a Dirac relativistic formulation of the ns^2 - $nsnp$ transition, the line strengths can be specified in terms of the $J \rightarrow \frac{1}{2}-\frac{3}{2}$ and $J \rightarrow \frac{1}{2}-\frac{1}{2}$ radial dipole transition matrix elements R_{31} and R_{11} by

$$S_r(\text{Res}) \equiv S(\text{Res})/\cos^2(\theta - \xi), \quad (9)$$

$$S_r(\text{Int}) \equiv S(\text{Int})/\sin^2(\theta - \xi), \quad (10)$$

where

$$\tan \xi \equiv \sqrt{2}(R_{31} - R_{11})/(2R_{31} + R_{11}). \quad (11)$$

Thus, with these corrections, the combined data base for the resonance and intercombination lines can be used to predict line strengths for both transitions for the entire isoelectronic sequence.

3.3. Inert-gaslike systems

The cases discussed above involve intrashell $\Delta n = 0$ transitions (ns - np for alkali-metallike sequences, ns^2 - $nsnp$ for alkaline-earthlike sequences) and the next logical step would be to extend the formalism to $\Delta n > 0$ transitions. Unfortunately this is not generally possible because almost no measured transition probability data exist for $\Delta n > 0$ transitions in multiply charged ions [1]. This is a consequence of the fact that decay rate data for multiply charged ions consist almost exclusively of lifetime measurements. These can be used to deduce transition probabilities, oscillator strengths, and line strengths for unbranched decays, but virtually no branching fraction measurements exist for multiply charged ions.

An unbranched set of intershell transitions exists for inert-gaslike systems, such as the $2p^6$ 1S_0 - $2p^53s$ 1,3P_1 transitions in the Ne sequence. Here the first excited state is extrashell, giving rise to unbranched $\Delta n = 1$ resonance and intercombination transitions. Here again the data have been found to converge toward the hydrogenic limit at high Z . In addition, the locus of points for the resonance and intercombination lines are virtually congruent, so that a measurement of one improves the knowledge of the other. The linearity and the congruency of two related transitions has been confirmed by *ab initio* calculations.

As a result of the increased effect of the λ^3 factor because of the intershell nature of the transition, the lifetimes for the inert-gaslike transitions decrease with Z much more severely than those of an intrashell alkaline-earthlike system. At high Z inert-gaslike lifetimes are too short to be measured by time-of-flight methods, and too long to be accessible to line width measurements. Thus the ability to extrapolate the available data to high Z is extremely valuable.

4. Transition probabilities and branching fractions

4.1. The need for branching fractions

Branching fractions are required to convert lifetime data to emission transition probabilities and absorption oscillator strengths. These quantities are needed, *e.g.*, to deduce elemental abundances from astrophysical spectra, to determine impurity concentrations from fusion plasma spectra, and to make transition-by-transition comparisons between experiment and theory.

As indicated in Section 3, lifetime measurements can be transformed to a slowly-varying isoelectronic systematization by reducing each one to its corresponding effective line strength factor. This regularity does not occur for the raw measurements, since the reciprocal lifetime of a branched decay is a sum of transition probabilities, each with a different wavelength dependence that contains a separate implicit dependence on Z . Thus, while branched line strength factors exhibit a simple and slowly varying isoelectronic behavior, lifetimes usually have a rapid isoelectronic variation containing many different powers of Z . The line strength reduction requires knowledge of the branching fractions.

Much progress has been made in the determination of branching fractions in neutral and singly ionized atoms through the use of absolute emission, absorption, or dispersion measurements, or through combined measurements of relative branching ratios and lifetimes [11]. In highly ionized atoms, many measurements of lifetimes in the 1-5% accuracy range have been made by ANDC analysis [12] of beam-foil measurements. However, as stated earlier, branching ratio measurements in multiply charged ions are virtually non-existent [1].

The reasons for this lack of data are clear. The measurement of branching ratios requires an intensity calibration of the detection equipment as a function of wavelength, which is difficult for multiply charged ions. Until recently, beam-foil excitation was the only general way of accessing highly ionized systems. With fast ion beam methods there are Doppler broadenings and shifts, polarizations due to anisotropic excitation, wavelengths that preclude reflective and transmissive optical elements, differential downstream decays and repopulations of the levels, *etc.* These features are ill-suited to standard methods for calibrating grating spectrometers and detection systems using laboratory-fixed standard lamps. It is now possible to supplement time-resolved beam-foil studies with measurements of relative intensities from a common upper level using ECR sources, ion traps, and high effect lasers, coupled to both grating and FTS spectrometers, but many similar problems in calibration must also be overcome with these methods.

4.2. Branching fractions from intermediate coupling amplitudes

When branching is within a multiplet between two complexes that are each dominated by a single configuration, branching fractions can be empirically specified from intermediate coupling amplitudes deduced from spectroscopic energy level data.

Because of its formulation in terms of a primary effective central (but non-Coulomb) potential with only secondary corrections for noncentral contributions, radial transition matrices are usually computed using wave functions obtained from the central approximation. If CI is present, the mixing is level dependent, and the radial transition element for each line in the multiplet must be separately considered. If CI is not present, and both the upper and the lower complex of the multiplet

Table I. Semiempirical (S) and measured (M) branching fractions for ns^2np^2 – ns^2nnp 's transitions in neutral atoms.

Transition	Branching fractions (%)					
	Si I		Ge I		Sn I	
	S	M	S	M	S	M
$^3P'_0 \leftarrow ^3P'_1$	33.3	33.3(3)	31.2	32.5(16)	32.3	27
$^3P_1 \leftarrow$	24.7	24.7(4)	21.2	22.1(11)	17.5	17
$^3P'_2 \leftarrow$	41.1	40.7(4)	38.1	37.1(19)	39.7	39
$^1D_2 \leftarrow$	0.88	1.2(1)	8.8	8.1(8)	10.0	17
$^1S'_0 \leftarrow$	0.06	<0.20(6)	0.52	0.23(2)	0.5	–
$^3P_1 \leftarrow ^3P_2$	25.2	24.6(3)	26.4	27.2(14)	28.3	22
$^3P'_2 \leftarrow$	74.8	74.5(3)	73.1	72.1(14)	68.5	71
$^1D'_2 \leftarrow$	0.02	0.027(4)	0.53	0.72(7)	3.2	7
$^3P'_0 \leftarrow ^1P'_1$	0.24	0.30(2)	2.9	4.6(5)	4.2	8
$^3P_1 \leftarrow$	0.25	0.20(2)	3.3	3.6(4)	6.8	4
$^3P'_2 \leftarrow$	0.15	0.20(2)	1.0	1.68(17)	0.01	–
$^1D'_2 \leftarrow$	92.0	93.4(2)	86.2	86.1(14)	82.2	88
$^1S'_0 \leftarrow$	7.4	5.7(12)	6.6	4.0(4)	6.8	–

is dominated by a single configuration, the radial transition moment can be eliminated from the specification of the branching fractions. Since the number of measured energy levels usually exceeds the number of IC amplitudes needed to describe them, the validity of the single configuration model can be easily tested.

4.3. Application: Si, Ge, and Sn sequences

A test of this approach to the ns^2np^2 – ns^2nnp 's transitions in the neutral atoms Si I, Ge I, and Sn I has been carried out [13, 14]. Since there are seven energy levels splittings (among the $^3P_{0,1,2}$, 1D_2 , 1S_0 in the ground configuration and among the $^3P_{0,1,2}$, 1P_1 in the excited configuration) that are described by four Slater parameters (F_2 , ζ_{pp} and G_1 , ζ_p), the overdetermination was used to test the single configuration assumption. This indicated that both the lower and upper manifolds are essentially pure configurations. The mixing angles θ_0 , θ_2 and θ_1 were deduced from the Slater parameters, and used to obtain the branching fractions predicted by these mixing angles in the context of the single configuration model. These results are displayed in Table I.

For these three neutral atoms, accurate experimental measurements of the branching fractions exist (cf. [13, 14]). These are also displayed in Table I. The semiempirical results agree nearly perfectly within the accuracies of the experimental measurements.

This agreement provides confidence that similar accuracy can be attained by extending these semiempirical calculations to singly and multiply charged ions in these isoelectronic sequences. Calculations have been carried out in the Si sequence for P II – Ar V [13], in the Ge sequence for As II – Br IV [13], and in the Sn sequence for Sb II – Cs VI [14]. Owing to the lack of measured branching fraction data for multiply-charged ions in the ultraviolet (UV), these results represent a valuable source of UV line calibration standards.

In the case of the Sn sequence, the mixing angles obtained from these Slater and spin-orbit parameters are empirically linear when displayed on a plot of $\cot(2\theta_j)$ vs $1/(Z-47)$. The branching fractions deduced from this mixing angle data for the Sn-like multiply charged ions Te III – Xe V are presented in Table II, together with their wavelengths. If the lifetimes of the upper

Table II. Wavelengths and semiempirical branching fractions (in %) for the $5s^25p^2$ – $5s^25p6s$ transitions in multiply charged ions of the Sn sequence.

Transition	Te III		I IV		Xe V	
	$\lambda(\text{\AA})$	B_{if}	$\lambda(\text{\AA})$	B_{if}	$\lambda(\text{\AA})$	B_{if}
$^3P'_0 \leftarrow ^3P'_1$	928.3	29.2	666.3	30.0	512.8	31.1
$^3P_1 \leftarrow$	971.2	15.0	698.0	15.3	538.6	16.1
$^3P'_2 \leftarrow$	1004.4	46.7	718.9	49.0	552.9	50.0
$^1D'_2 \leftarrow$	1106.6	8.2	784.0	5.0	600.4	2.4
$^1S'_0 \leftarrow$	1293.2	0.9	885.7	0.7	664.8	0.4
$^3P_1 \leftarrow ^3P_2$	893.2	27.7	649.3	27.6	500.6	27.6
$^3P'_2 \leftarrow$	921.2	61.7	667.3	57.8	513.0	54.3
$^1D'_2 \leftarrow$	1006.4	10.7	723.0	14.6	553.5	18.1
$^3P'_0 \leftarrow ^1P'_1$	848.9	2.6	619.7	1.5	469.2	0.7
$^3P_1 \leftarrow$	884.7	6.0	647.0	5.2	490.6	4.3
$^3P'_2 \leftarrow$	912.2	2.0	664.9	5.2	502.6	9.4
$^1D'_2 \leftarrow$	995.7	77.3	720.2	74.8	541.4	71.6
$^1S'_0 \leftarrow$	1144.2	12.1	805.1	13.3	593.3	14.1

levels of these ionic transitions could also be measured (to test the constancy of the interconfigurational transition moment that occurs in the nonrelativistic Schrödinger approximation), additional intensity ratios among the three multiplets could be established. Thus, by utilizing IC relationships obtained from spectroscopic data in a system possessing little CI, a set of calibration standards can be obtained. These can then be utilized to measure branching ratios in systems of greater configurational complexity.

5. Future directions

Much progress has been made in the measurement of lifetimes in a wide variety of atomic and ionic systems. However, to obtain the comprehensive atomic data base needed for user applications and to test theoretical methods, it is essential that transition probabilities and oscillator strengths for excited states with branched decays be systematically determined. Energy level and oscillator strength data provide a primary basis set for free atoms that can be used to specify their behavior in more complex environments. These quantities are commonly used to compute adiabatic and nonadiabatic electrostatic polarizabilities, interaction cross sections, indices of refraction, and many other properties of bulk matter. Unfortunately, various fields within physics are often fragmented within their levels of complexity, whereby each speciality deals with its own set of “fundamental particles,” rather than building on the data base of systems of lower complexity. A comprehensive data base for use with modern high performance computational capabilities is needed if atomic physics is fulfill its role as an “enabling science.”

Clearly one of the significant problems for the future involves the development of intensity calibration standards of line radiation in the UV region for use in calibrating detection equipment, and the use of these standards for making comprehensive measurements of branching fractions for transitions in multiply charged ions.

References

1. Curtis, L. J., “Precision Oscillator Strengths and Lifetime Measurements”, in *Atom. Molec. & Opt. Phys. Ref. Book*, (ed. G. W. F. Drake), (AIP Press, NY, 1996) pp. 206–212.

2. Curtis, L. J. and Martinson, I., "Lifetimes of Excited States in Highly Charged Ions", in *Atomic Physics with Heavy Ions*, (eds. H. F. Beyer and V. P. Shevelko), (Springer, Berlin, 1999) pp. 197–218.
3. Curtis, L. J., "Atomic Structure and Lifetimes: A Conceptual Approach", (Cambridge University Press, 2003).
4. Edlén, B., *Physica Scripta* **17**, 565 (1978).
5. Curtis, L. J., Ellis, D. G. and Martinson, I., *Phys. Rev. A* **51**, 251 (1995).
6. Schweppe, J. *et al.*, *Phys. Rev. Lett.* **66**, 1434 (1991).
7. Johnson, W. R., Liu, Z. W. and Sapirstein, J., *At. Data Nucl. Data Tables* **64**, 271 (1996).
8. Chou, H.-S. and Johnson, W. R., *Phys. Rev. A* **56**, 2424 (1997).
9. Curtis, L. J., *Phys. Rev. A* **40**, 6958 (1989).
10. Curtis, L. J., Ellis, D. G., Matulioniene, R. and Brage, T., *Physica Scripta* **55**, 240 (1997).
11. Sikström, C. M., Nilsson, H., Litzén, U. and Lundberg, H., *J. Quant. Spectrosc. Radiative Transfer* **74**, 55 (2002).
12. Curtis, L. J., Berry, H. G. and Bromander, J., *Phys. Lett. A* **34**, 169 (1971).
13. Curtis, L. J., *J. Phys. B* **31**, L769 (1998); **33**, L259 (2000).
14. Curtis, L. J., *Physica Scripta* **63**, 104 (2001).